CSIRO PUBLISHING www.publish.csiro.au/journals/eg Copublished paper, please cite all three:
Exploration Geophysics, 2011, **42**, 58–68; *Butsuri-Tansa*, 2011, **64**, 58–68; *Jigu-Mulli-wa-Mulli-Tamsa*, 2011, **14**, 58–68

Monitoring and detecting CO_2 injected into water-saturated sandstone with joint seismic and resistivity measurements

Jongwook Kim[1,3] Toshifumi Matsuoka[1] Ziqiu Xue[2]

[1]Laboratory of Environment and Resource System Engineering, Department of Urban Management, Graduate School of Engineering, Kyoto University, Kyodai-Katsura, Nishikyo, Kyoto 615-8540, Japan.
[2]Research Institute of Innovative Technology for the Earth, 9-2 Kizugawadai, Kizu, Kyoto 619-0292, Japan.
[3]Corresponding author. Email: gplkim@earth.kumst.kyoto-u.ac.jp

Abstract. As part of basic studies of monitoring carbon dioxide (CO_2) storage using electrical and seismic surveys, laboratory experiments have been conducted to measure resistivity and P-wave velocity changes due to the injection of CO_2 into water-saturated sandstone. The rock sample used is a cylinder of Berea sandstone. CO_2 was injected under supercritical conditions (10 MPa, 40°C). The experimental results show that resistivity increases monotonously throughout the injection period, while P-wave velocity and amplitude decrease drastically due to the supercritical CO_2 injection. A reconstructed P-wave velocity tomogram clearly images CO_2 migration in the sandstone sample. Both resistivity and seismic velocity are useful for monitoring CO_2 behaviour. P-wave velocity, however, is less sensitive than resistivity when the CO_2 saturation is greater than ~20%. The result indicates that the saturation estimation from resistivity can effectively complement the difficulty of CO_2 saturation estimations from seismic velocity variations. By combining resistivity and seismic velocity we were able to estimate CO_2 saturation distribution and the injected CO_2 behaviour in our sample.

Key words: Berea sandstone, carbon dioxide (CO_2) storage, CO_2 saturation, P-wave velocity, resistivity, seismic tomography.

Introduction

Greenhouse gases, a main cause of global warming, are a serious issue in various countries around the world. As global warming is a serious problem, reduction technologies for CO_2, the most abundant greenhouse gas, have become urgent business. In 1997, the Kyoto Protocol defined an implementation goal that most of the world's countries should reduce CO_2 by 5.2% of 1990 totals. Currently, trading of carbon credits are seen to be one way to meet the goals of the Kyoto Protocol. In European Union (EU) countries, CO_2 credit trades are executed in earnest and technologies such as Carbon Capture and Storage (CCS) have become an important topic of discussion. Geological sequestration is thought as an effective way to mitigate greenhouse gas emissions. Geological sequestration can be classified by methods such as disposal into the deep sea as a hydrate, injection into saline aquifers or depleted oil or gas fields, and adiabatic underground injection. The sequestration of carbon dioxide (CO_2) in saline aquifers has been proposed as an effective and advanced technology. To ensure the safety and effective storage of CO_2 sequestration, it is necessary to monitor injected CO_2 in the subsurface, and to quantify the mass of CO_2 in reservoirs.

Geophysical surveys play an important role in CO_2 monitoring. Seismic surveys have shown great results at sites in Sleipner, Weyburn, and Nagaoka (Bunge, 2000; Arts et al., 2002, 2004; Davis et al., 2002; Xue et al., 2006). At the Nagaoka pilot site, time-lapse induction and sonic logging successfully detected CO_2 breakthrough at two observation wells, and monitored the behaviour of injected CO_2 in the permeable zone of the reservoir (Xue et al., 2006). Experiments have been conducted in the laboratory to monitor resistivity or seismic velocity while injecting supercritical CO_2 into various sandstones under in-situ reservoir conditions (Xue et al., 2002, 2005; Xue and Ohsumi 2004*a*, 2004*b*, 2005; Onishi et al., 2006; Kim et al., 2009; Nakatsuka et al., 2009).

Seismic surveys provide the most attractive approach for obtaining the spatial coverage required for mapping the location and movement of CO_2 in the subsurface. Crosswell seismic surveys has been successfully applied to map the movement of injected CO_2 at the Nagaoka and Frio pilot sites (Xue et al., 2005; Saito et al., 2006; Daley et al., 2007). Seismic tomography is efficient for imaging CO_2 migration in reservoirs. Gassmann's theory is often used to estimate CO_2 saturation from seismic velocity (Gassmann, 1951). From sonic and resistivity logging results, P-wave velocity becomes less sensitive when CO_2 saturation is greater than 20%, while the resistivity keeps increasing with increasing CO_2 saturation (Nakatsuka et al., 2008; Kim et al., 2009). P-wave velocity is not sensitive to gas saturation in high gas saturation regimes (>20%) for either homogenous saturation or patchy saturation with patch sizes much smaller than a wavelength (Xue and Lei, 2006; Lei and Xue, 2009). From this result, when saturation becomes more than 20%, the variation in P-wave velocity becomes too weak for estimating CO_2 saturation quantitatively. In order to overcome the weak point of seismic monitoring for estimating CO_2 saturation, resistivity monitoring is considered.

In this paper, we report laboratory experiments conducted to measure resistivity and P-wave velocity changes simultaneously, while injecting supercritical CO_2 into water-saturated sandstone. For better understanding of the relationship between P-wave velocity or resistivity and CO_2 saturation, P-wave velocity and resistivity changes associated with CO_2 migration in a porous

 10.1071/EG11002 0812-3985/11/010058

structure were determined. Here, we also present field results obtained from the Nagaoka pilot site.

Sample and experimental details

A cylindrical sample of Berea sandstone (50 mm in diameter and 100 mm in length, 19% porosity) is utilised in the study. Figure 1 shows the configuration of piezoelectric transducers and electrodes attached to the Berea sandstone for seismic velocity and resistivity measurements, respectively. The figure indicates the zone utilised for resistivity measurements as well as a diagram of ray paths for P-wave velocity measurements and P-wave velocity tomography.

Two flat current electrodes, 50 mm in diameter, were attached at the top and the bottom of the sample, and four ring-shaped potential electrodes of 2.5 mm width were attached to the sample's surface at a spacing of 25 mm. These electrodes are made of copper mesh coated with silver, which to avoid corrosion due to contact with acid.

For seismic velocity monitoring, eight transducers (ch 1–8) as transmitters are attached on one side of the sample and another eight transducers (ch 9–16) are on the other side of the sample as receivers (Figure 1). Each piezoelectric transducer has a characteristic frequency of 1 MHz. Stainless steel end pieces are attached to both ends of the sample, and a grooved plate is placed between the end piece and the sample at either end. Concentric grooves connected by radial grooves are carved onto the plate surface to enable uniform CO_2 injection over the entire surface of the sample's end. Nylon mesh is put between the end piece and the current electrode for insulation. The sample assembly is then sealed with silicon sealant, ~5 to 10 mm in thickness, to prevent the leakage of CO_2 from the sample and also to prevent the infiltration of oil (used as a hydrostatic pressure medium) into the sample.

The experimental apparatus consists of the injection system, pressure vessel, resistivity and seismic measurement equipment, and data recording system. Figure 2 shows a simplified configuration of experimental equipment in this study. To simulate temperature and pressure conditions in deep saline reservoirs, the sample is set into a high-pressure vessel. Three syringe pumps are used to control the confining pressure, the pore pressure, and the injecting CO_2 pressure, respectively. A syringe pump for confining pressure is utilised to keep the hydrostatic pressure constant. A syringe pump for pore pressure is utilised to keep the pore pressure (back pressure) constant at the top end, and is set to reduce the pre-pressure build-up, which can be caused by CO_2 injection. A syringe pump for CO_2 is utilised to inject the CO_2 from the bottom end of the sample at a pre-set constant pressure. The temperature is controlled with a band heater covering the surface of the vessel.

The experimental procedures for CO_2 injection under in-situ conditions in a reservoir involved the following steps. After placing the sample in the pressure vessel, the pressure is increased to 13 MPa under hydrostatic pressure conditions. The sample is then saturated with a KCl solution with a resistivity of 1 Ω.m. The pore pressure is increased to 10 MPa and is kept constant during CO_2 injection. Supercritical CO_2 is injected into the water-saturated sandstone at 10.5 MPa. To ensure that the injected CO_2 is in the supercritical phase, the temperature is set at 40°C.

Waveforms of electric potential and P-waves were recorded at every 3 min during CO_2 monitoring. Figure 3 shows an example of recorded waveforms for the electric potential and the compressional wave obtained before and after CO_2 injection. CO_2 injection causes an increase of electric potential (Figure 3*a*), and an increase in traveltime and higher damping in P-wave propagation.

Experimental results and discussion

As shown in Figure 1, the main body of the Berea sandstone sample is divided into three zones (zones 1–3). Figure 4 shows changes in resistivity, P-wave velocity and amplitude during the CO_2 injection (and drainage). When CO_2 is injected into a sample, pore water in the sandstone will be partially displaced by CO_2.

Figure 4*a* shows the resistivity changes obtained in the three zones during injection of supercritical CO_2 from the bottom of the sample. CO_2 injection started at 0 min. Resistivities of the lower (zone 1), middle (zone 2), and upper (zone 3) parts of the sample are shown in different colours. The resistivity for the initial water-saturated condition ranged from 12.5 to 13.6 Ω.m, while the resistivity increased due to CO_2 substitution for pore water, consequently ranging from 23 to 33 Ω.m in zones 1–3.

Figure 4*b* shows the P-wave velocity and amplitude obtained along the eight shortest paths during injection. P-wave velocities are measured directly from the arrival times, and amplitudes are

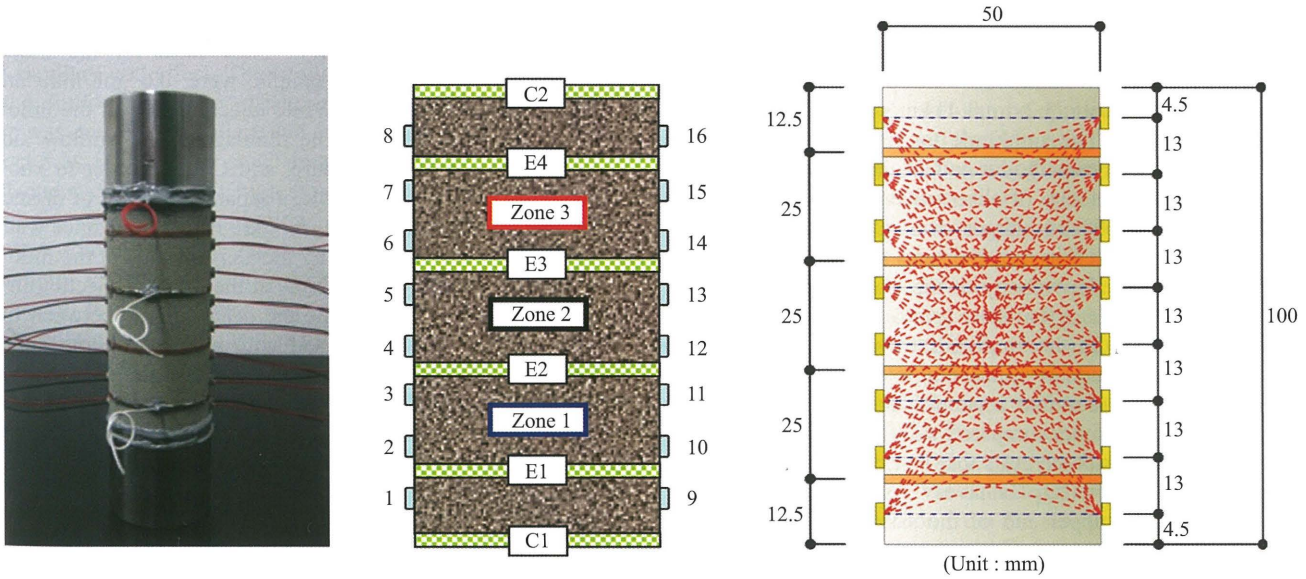

Fig. 1. Configuration of piezoelectric transducers and electrodes with a Berea sandstone sample (Kim et al., 2009).

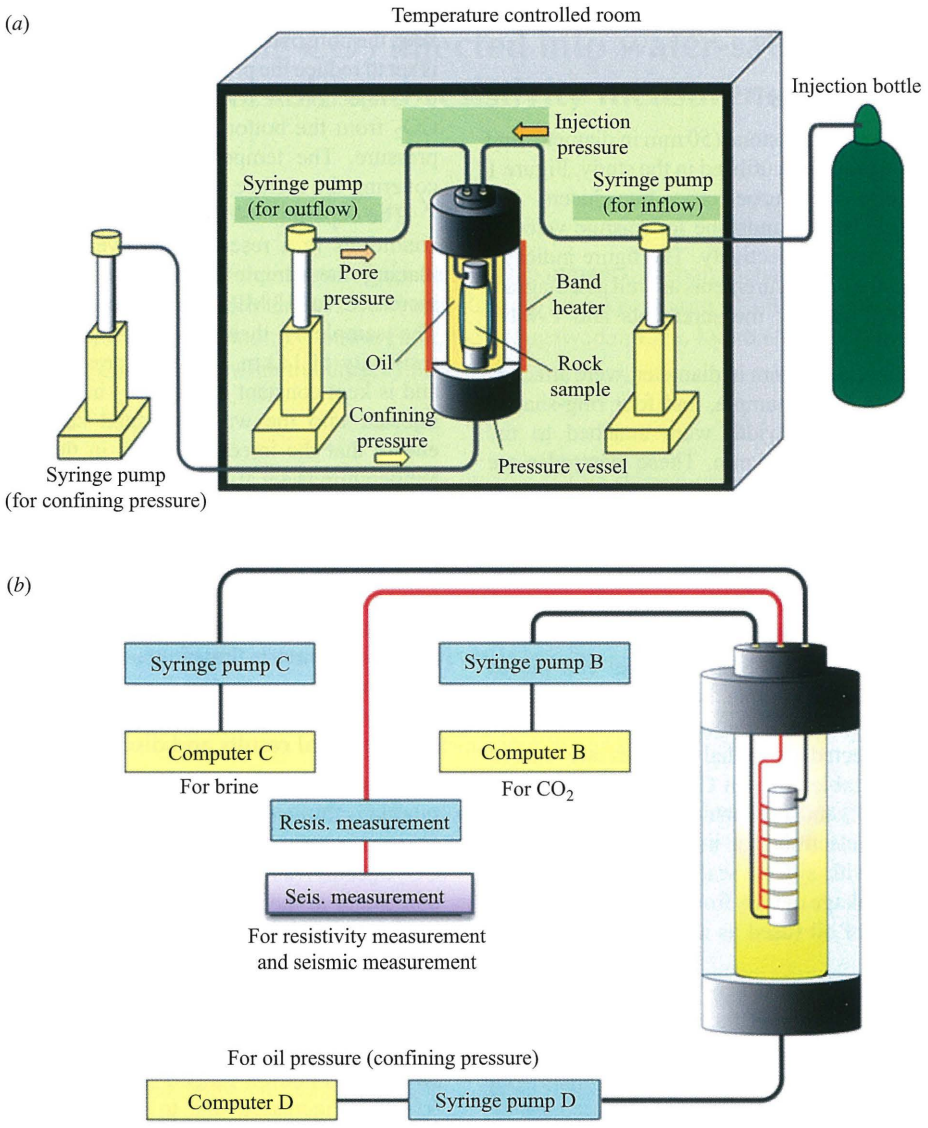

Fig. 2. Configuration of (*a*) the experimental apparatus and (*b*) the measurement system (Kim et al., 2009).

measured as the maximum magnitude of the observed waveforms. When the front face of migrating CO_2 reaches a ray path, a significant decrease is observed in the P-wave velocity and amplitude along that path. The P-wave velocity for the initially water-saturated condition ranged from 3.51 to 3.71 km/s, and the velocity for the partial CO_2-saturated sandstone ranged from 3.2 to 3.41 km/s at eight ray paths (ch 1–9 ~ch 8–16). The amplitude for the first arrival of the P-wave decreased drastically due to CO_2 injection. Comparing the amplitude and velocity of observed P-wave, the amplitude decrease (average 63%) is larger than the velocity decrease (8% in average), which in turn indicates that the amplitude is more sensitive than the velocity to the characteristics of pore fluid. The result indicates that there is an advantage in detecting CO_2 in a sample from the amplitude than from the velocity. However, the amplitude is impossible to monitor over a long period of CO_2 migration into a sample, due to rapid reduction of a change in amplitude, compared with a change in velocity. Therefore, such a result suggests that P-wave velocity is useful for monitoring how CO_2 behaves. As the injected CO_2 moves towards the upper end of the sample, the changes in resistivities and P-wave velocities and amplitudes get smaller. The magnitudes of measured results are reduced because the amount of injected CO_2 is small, as a fingering type of CO_2 movement took place from the bottom of the sample due to gravity.

Figure 5 shows flow rates and volumes at the inflow and outflow sides against CO_2 injection time for the experiment. CO_2 injection started at 0 min. Flow rates for the inflow and outflow sides of the sample were 0.05 mL/min and –0.05 mL/min, respectively. While injecting CO_2 at the inflow side, the order of fluids in the drainage at the outflow side was water, a water/CO_2 mixture, and CO_2. In order to know the volumes of CO_2 in a sample, a separate analysis of drained water and a drained water/CO_2 mixture is required, since water at the outflow side is drained by the CO_2 injected at the inflow side. In order to know the volume at the time of injection in a sample one needs to determine the dead volume between the pipeline of fluid flow connected with a syringe pump and a pressure vessel at the bottom of the sample at the CO_2 injection point. The dead volume can be calculated as the time difference between the start time of the injection of CO_2 and the initial time of P-wave velocity change at the first set of transducers (ch 1–9) attached at the lowest point of the sample surface (Figure 6). In this experiment, the total volume of the sample was 196.25 mL, and the pore volume was 37.3 mL. The dead volume was 5.1 mL. Figure 6 shows changes in resistivity for the three zones and the changes in

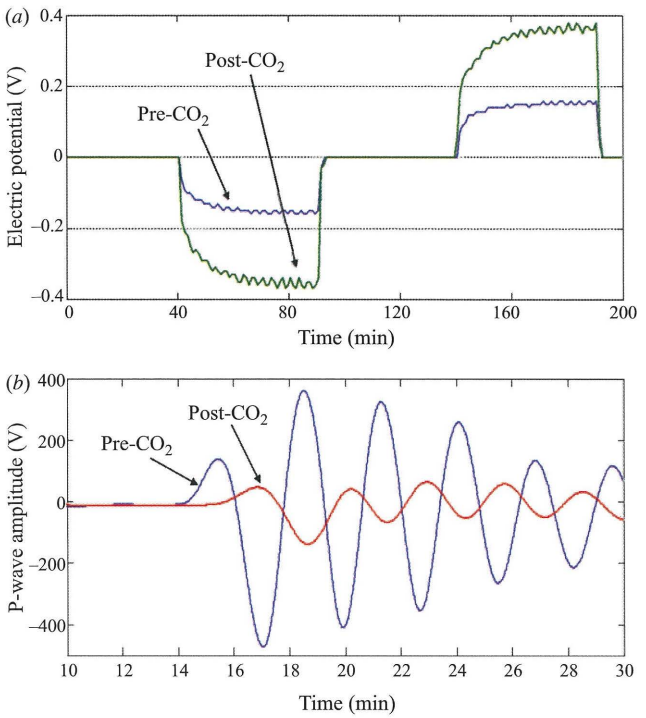

Fig. 3. (*a*) Electric potential for resistivity and (*b*) the measured P-wave for seismic tomography, before and after CO_2 injection.

P-wave velocity for eight ray paths against injected volumes after starting CO_2 injection.

Figure 7 shows the average P-wave velocity and the resistivity measured at zones 1–3 against CO_2 saturation. CO_2 saturation was calculated from the pore volume in the pore space of a sample divided into the injected CO_2 volume, ignoring the dead volume. The resistivity changed when CO_2 was saturated, by up to 37% at zone 1, up to 33% at zone 2, and up to 18% at zone 3. The P-wave velocity became less sensitive when the CO_2 saturation was not less than ~20%, generally in zones 1–3. Resistivity showed a monotonous increase with increasing CO_2 saturation when the CO_2 saturation was not more than ~20%. These results suggest that electric monitoring could be utilised as a monitoring method.

As seen in Figure 7, during injection, the change in resistivity did not continue after CO_2 saturation reached ~18% at zone 3. Furthermore, the resistivity response was delayed and the resistivity variation was small by comparison with zones 1 and 2. The non-uniform saturation profile at steady-state is called the capillary end effect. The capillary end effect was observed at the outflow face. The variation of CO_2 saturation along the core was due to the capillary end effect at the outflow end. This effect was found to be small in relatively long porous cores and under conditions of high flow rates and leads to a more uniform saturation distribution. Capillary end effects can explain some resistivity variations in zone 3, compared with resistivity variations in zones 1 and 2 due to CO_2 saturation. However, P-wave velocity variations cannot be explained by the capillary end effect, as it is difficult to distinguish changes in velocity-saturation in zones 1–3. It is necessary to estimate uniform saturation or non-uniform saturation from P-wave velocity based on the theories of Gassmann fluid substitution. In the future, a study will be conducted to explain capillary end effects with the purpose of better understanding the relationship between the CO_2 saturation distribution and P-wave velocity.

Figure 8 shows reconstructed P-wave velocity images during the injection of supercritical CO_2 in Berea sandstone, using time-lapse seismic tomography, indicating the distribution of P-wave velocity changes at selected time intervals during injection. In this case, the upward CO_2 migration in the sample was clearly imaged. The injection of supercritical CO_2 in this sample clearly caused the distribution of P-wave velocity changes along the profile. The common outcomes are summarised as follows: most parts of the profiles showed negative P-wave velocity changes, ranged from 0 to –0.4 km/s. After breakthrough of CO_2 at the top end, P-wave velocity continued to decrease slowly, and finally reached a stable level after 393 min for this Berea sandstone sample. During the injection, a P-wave velocity decrease appeared around the bottom end 123 min after starting injection (Figure 8). The area of negative P-wave velocity change expanded with increasing elapsed time, and reached the top end after 369 min.

Figure 8 also shows the distribution of the CO_2 saturation ratio versus CO_2 injection behaviour in the sample by comparing the relationship between the CO_2 saturation calculated using Archie's equation (Figure 9) and velocity images reconstructed using time-lapse seismic tomography. Tomographic images of VP change were reconstructed from differential travel times using difference tomography methods as outlined by Lei and Xue (2009). For CO_2 monitoring, we are more interested in the relative change of seismic velocity caused by CO_2 injection than the absolute velocity distribution. The effect of CO_2 injection on the P-wave velocities measured in the laboratory has been examined for CO_2 in the supercritical phase. By directly using differential arrival times, determined manually by the comparison of two consecutive waveforms along the same path, the differential tomography method is able to image the P-wave velocity change during injection of CO_2. Temporal-spatial distributions of relative velocity change were well imaged. Such distributions of P-wave velocity change reflect supercritical CO_2 migration in the water-saturated sample.

As seen in Figure 8, the reconstructed P-wave velocity tomogram images clearly showed CO_2 migration in the sandstone sample. It is also notable that the present experimental results show a wide distribution of the P-wave velocity change during CO_2 injection. The results indicate that the homogeneity of pore distribution plays an important role on governing CO_2 migration. This suggests that the migration of CO_2 in the rock sample is homogenous. Homogenous pore distribution or homogenous distribution of fluid flow channels may cause homogenous CO_2 migration. The results indicated the changes in resistivity and P-wave velocity associated with the movement of injected CO_2 in the pore structure. Seismic tomography results for monitoring CO_2 migration depend strongly on resistivity increases and velocity reductions caused by injecting CO_2. The result can be applied to simultaneously evaluate CO_2 saturation and the behaviour of CO_2 migration.

To overcome the weakness of seismic monitoring for estimating CO_2 saturation, there is a need for accurate estimation of CO_2 saturation using resistivity. A study was conducted as a part of basic studies with the purpose of better understanding how one should estimate the saturation of CO_2 during sequestration, using resistivity. All water-saturation determinations from resistivity in clean (non-shaly) formations with homogenous intergranular porosity are based on the most commonly and widely used water saturation equation as proposed by Archie (1942). The equation relates the resistivity of the formation to the porosity, the water saturation, and the resistivity of pore water. We considered the parameters needed to calculate CO_2 saturation from the resistivity result. Archie's equation is utilised to determine the CO_2 saturation:

$$R = \alpha \cdot \phi^{-m} \cdot S_w^{-n} \cdot R_w, \quad (1)$$

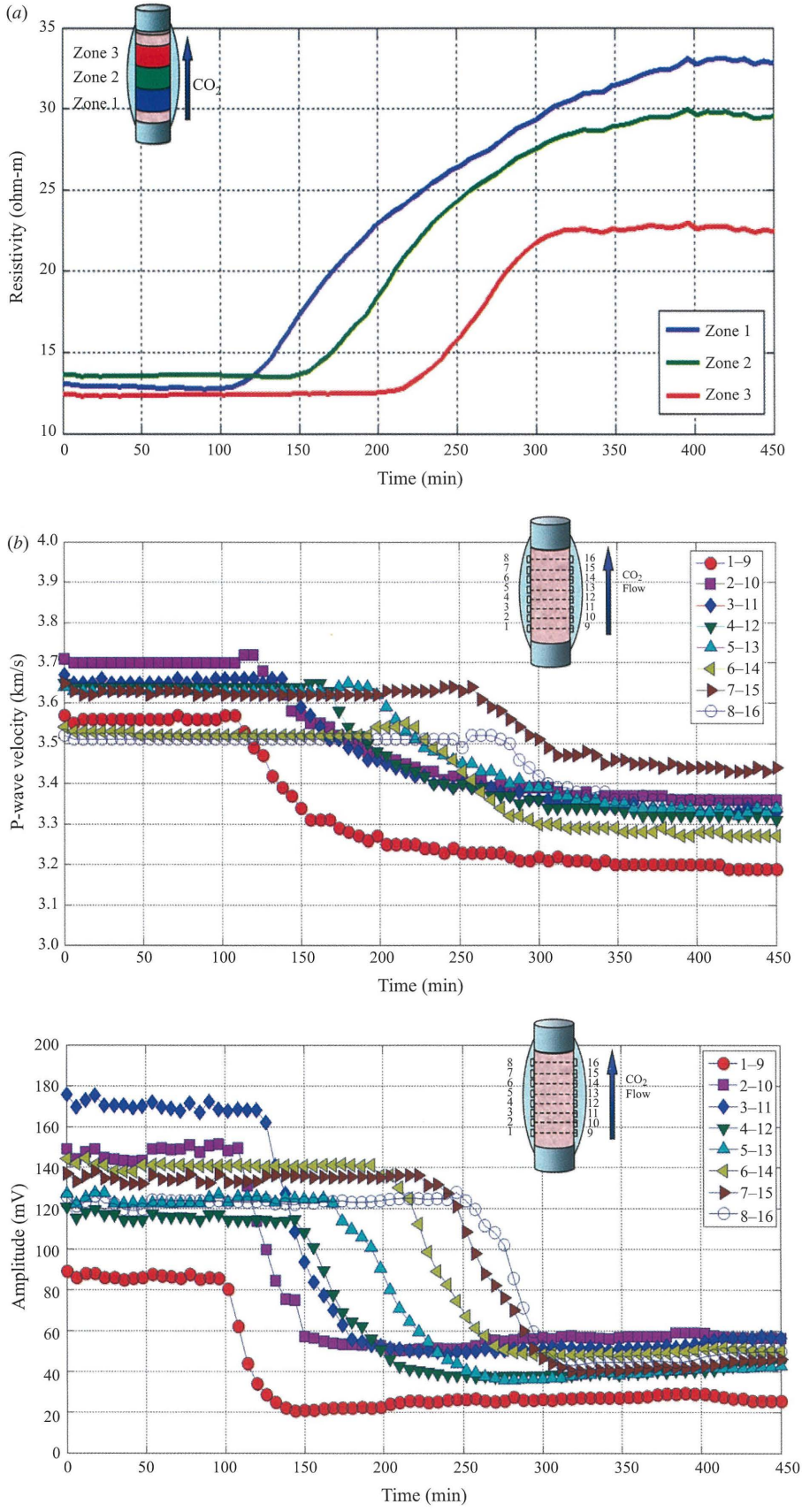

Fig. 4. Time variation in (*a*) resistivity and (*b*) seismic properties (velocity, amplitude) obtained while injecting supercritical CO_2 into water-saturated Berea sandstone.

where S_w is the water saturation (fraction), n is the saturation exponent (usually taken as equal to 2), R_w is the formation water resistivity (Ω.m), R is the true formation resistivity (Ω.m), and F is the formation factor ($F=\alpha\cdot\phi^{-m}$), where ϕ is the porosity, α is the cementation factor, and m is the cementation exponent. By transforming

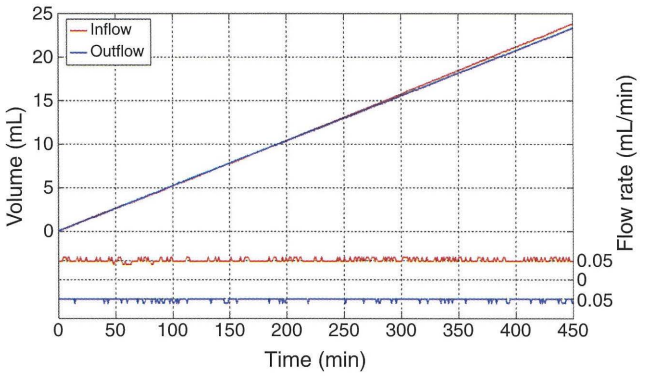

Fig. 5. Flow rates and volumes at the inflow and outflow sides plotted against CO_2 injection time during the experiment conducted with Berea sandstone.

equation 1, the saturation of CO_2 (S_{CO_2}) can be expressed as equation 2:

$$S_{CO_2} = 1 - S_w = 1 - \left(\frac{\alpha \cdot R_w}{R \cdot \phi^m}\right)^{\frac{1}{n}}. \quad (2)$$

Relevant parameters were provided from an experimental study and are the following: $a = 1$, $m = 1.59$, and $R_w = 1$. The porosity was measured in this study and was determined to be 0.19.

Figure 9 shows the CO_2 saturation as calculated by equation 2 from the resistivity results. CO_2 saturations increased by up to 37% at zone 1, by up to 33% at zone 2, and by up to 26% at zone 3. In the experiment, the CO_2 saturation calculated from resistivity using Archie's equation showed a good match with CO_2 saturation from the CO_2 volume injected into the water-saturated sandstone. For Berea sandstone, Archie's equation showed a good match with the real saturation estimated from replaced brine (Onishi et al., 2006).

As seen in Figures 4*a* and 9, the resistivity and CO_2 saturation increased due to CO_2 injection, but the resistivity and CO_2 saturation at zone 1 decreased a little in the early stages of injection. Before injecting CO_2 into a sample, the injecting CO_2 reacted with the injected water in the pipeline between the syringe pump and the bottom of the sample. When a little dissolved CO_2 reaches the electrode at zone 1, the resistivity at zone 1 decreased a little from the initial resistivity of water-saturated sandstone. The resistivity increased when the undissolved CO_2 reached zone 1 later. The CO_2 saturation calculated from the resistivity at zone 1 also become negative. The Nagaoka pilot CO_2 injection project provided a similar result, with an experimental result that confirmed the presence of dissolved CO_2 within the reservoir, as evidenced by low resistivity observed from induction logging after starting supercritical CO_2 injection (Xue et al., 2006). Furthermore, the results confirmed that the decrease in resistivity could provide a specific tool to detect dissolved CO_2 when water and CO_2 were reactive. In the longer term, the solubility and reactivity of the CO_2 will increase the stability of the storage with dissolution mechanism of trapped liquid CO_2. The results can provide the possibility to obtain a better understanding of dissolved CO_2 saturation distribution in a reservoir rock, and a monitoring tool may be able to detect dissolved CO_2 from changes in resistivity.

Figure 10 shows relationships between P-wave velocity and resistivity change against CO_2 saturation from (a) experiment results and (b) logging results from the Nagaoka site (Nakatsuka et al., 2008; Xue and Watanabe, 2008). In the experiment the CO_2 saturation of Berea sandstone calculated from resistivity using Archie's equation was very well matched with the CO_2 saturation from the injected CO_2 volume in sandstone with the same conditions of the reservoir. The experiment and the Nagaoka results showed similar responses when CO_2 saturation was less than roughly 20%, both the resistivity and the P-wave velocity are sensitive. However, when the CO_2 saturation was more than ~20%, the increase in resistivity showed constant sensitivity, while reduction of the P-wave velocity became less sensitive. The result indicates that the saturation estimation from resistivity can effectively complement the difficulty of over 20% CO_2 saturation estimations from seismic velocity variations.

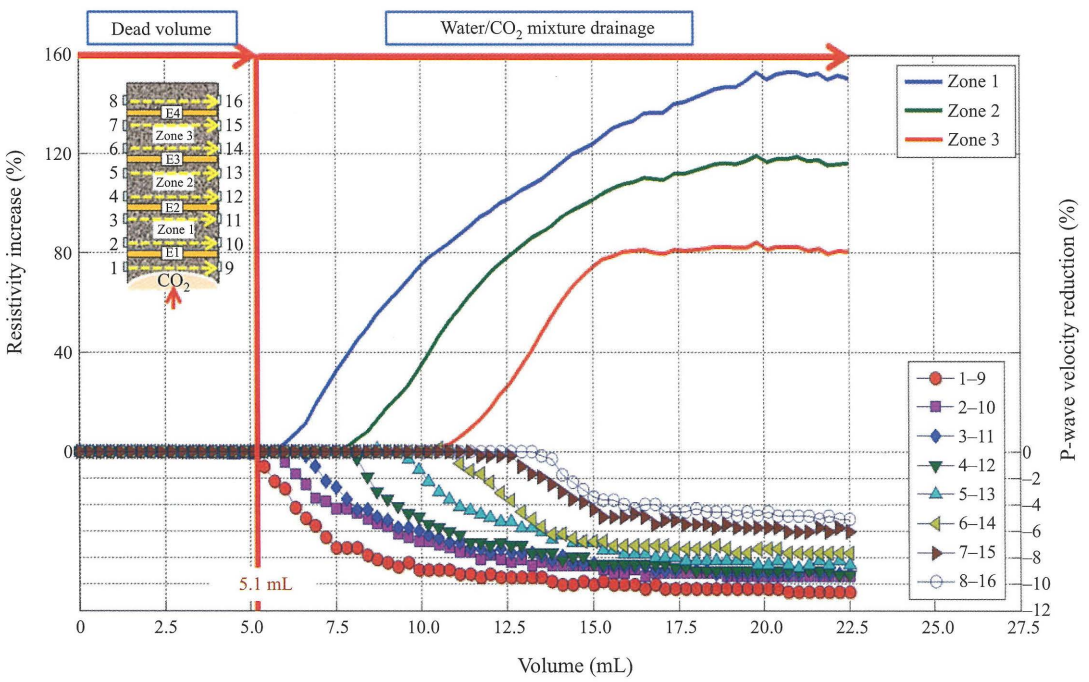

Fig. 6. Changes in the resistivity and P-wave velocities for the three zones and eight ray paths plotted against injection volume after a CO_2 injection.

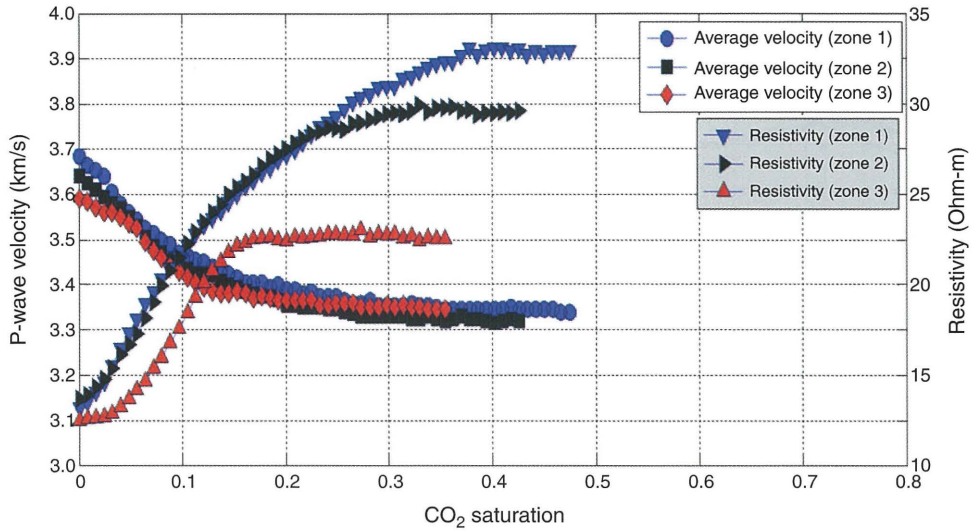

Fig. 7. Variations of P-wave velocity and resistivity plotted against CO_2 saturation calculated from CO_2 volume during the injection of supercritical CO_2 into water-saturated Berea sandstone.

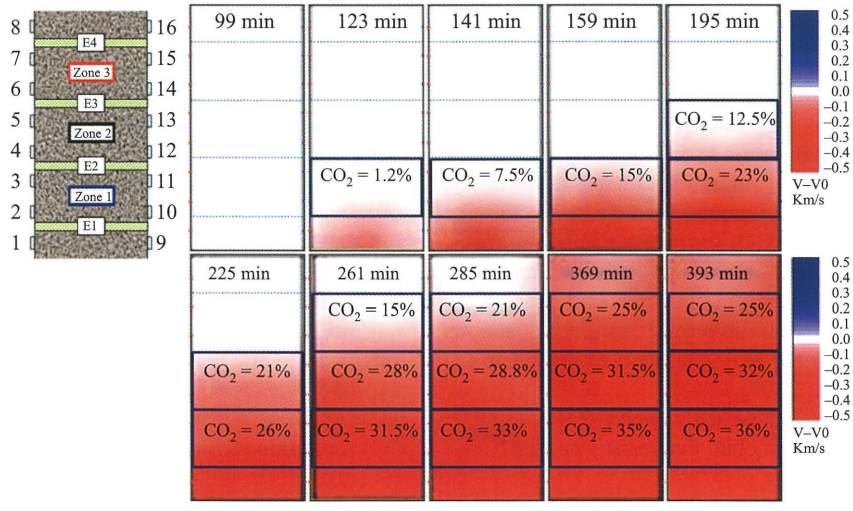

Fig. 8. The reconstructed velocity images and CO_2 saturation distributions from seismic tomography during the injection of supercritical CO_2 into Berea sandstone.

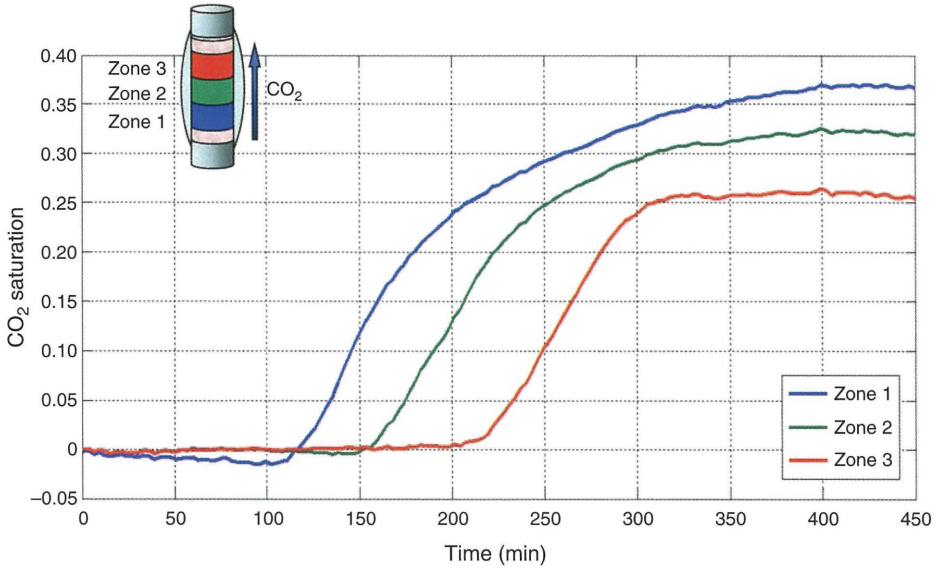

Fig. 9. CO_2 saturation from resistivity (calculated by Archie's equation) during CO_2 injection in water-saturated sandstone.

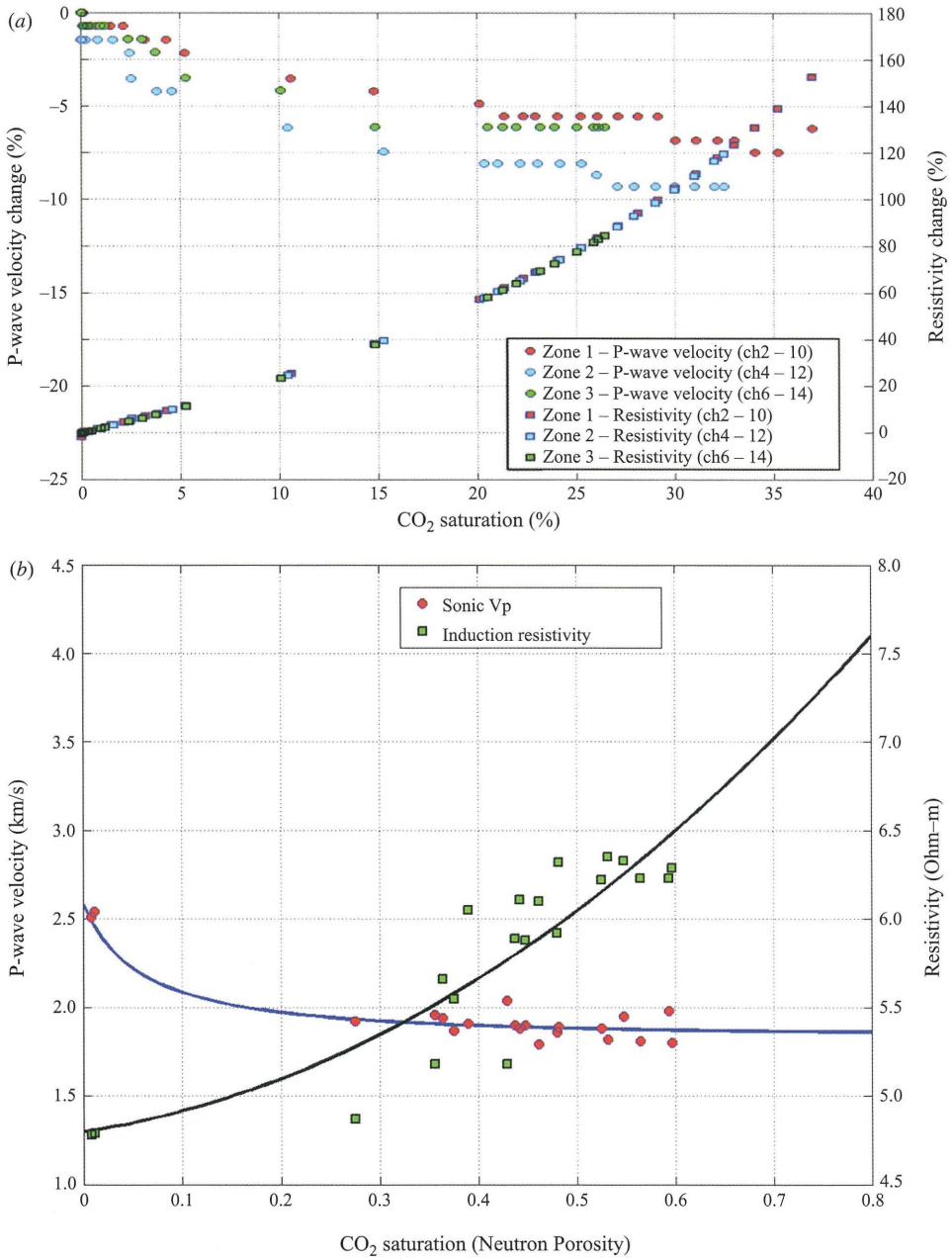

Fig. 10. (*a*) The relationship between P-wave velocity and resistivity change versus CO_2 saturation in the experiment; and (*b*) the relationship between P-wave velocity and resistivity change versus CO_2 saturation at the Nagaoka site (Xue and Watanabe, 2008; Nakatsuka et al., 2008).

Figure 11 provides the percentages for the resistivity increase and the P-wave velocity reduction as a combined resistivity and seismic velocity variation graph. The resistivity increase ranged from 80.5% to 152.9%, and the P-wave velocity reduction ranged from 5.4% to 10.6%. Resistivity increases and velocity reductions depend strongly on CO_2 migration. When the injected CO_2 reached each zone and path, the resistivity and velocity changed, beginning from zone1 and path ch 1–9.

As seen in Figures 4 and 11, we have confirmed CO_2 migration from the changes in P-wave velocity, amplitude, and resistivity when supercritical CO_2 was injected into water-saturated sandstone, and when CO_2 saturation increased due to CO_2 injection. When the front of migrating CO_2 reached the ch 1–9 ray path in the sample, the P-wave velocity decreased along that path after 106 min and the amplitude after 94 min. The results indicate that the amplitude change was faster than the P-wave velocity change when the front of migrating CO_2 reached a ray path. When the front of migrating CO_2 reached the ch 2–10 ray path, the P-wave velocity decreased along that path after 118 min and the amplitude after 106 min. When compared to the initial P-wave velocity and resistivity in zone 1, the resistivity increased by more than 0.6 Ω.m that of the initial resistivity, as the CO_2 saturation was 1% at that time. The resistivity change was slightly faster than the P-wave velocity change when the front of migrating CO_2 reached this ray path. When the front of migrating CO_2 reached the ch 4–12 ray path, the P-wave velocity decreased along that path after 162 min and amplitude after 144 min. When compared to the initial P-wave velocity and resistivity in zone 2, the resistivity increased by more than 1.2 Ω.m, as the CO_2 saturation was 2.4%. The resistivity change was slightly faster than the P-wave velocity change when the front of migrating CO_2 reached this ray path. When

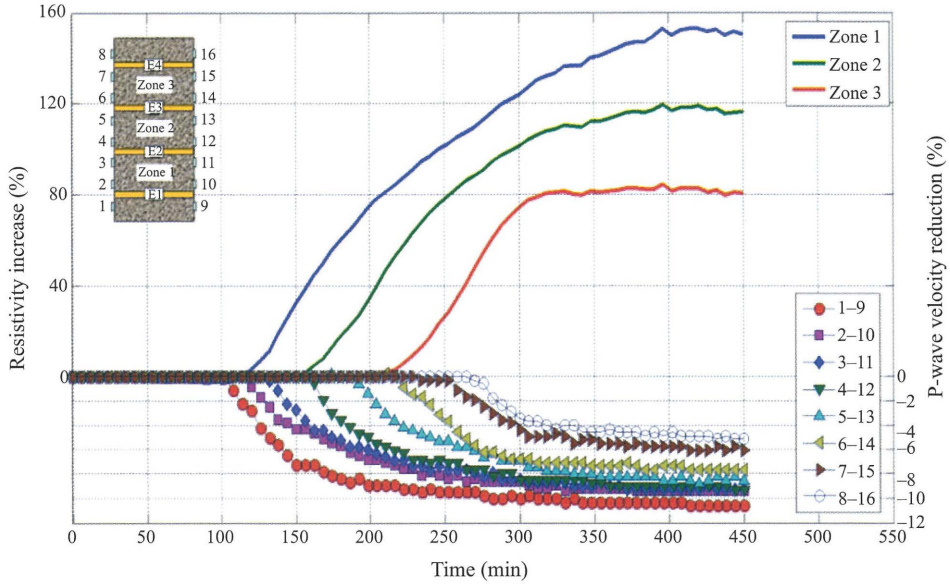

Fig. 11. The combined resistivity and seismic velocity change plotted against CO_2 injection.

the front of migrating CO_2 reached the ch 6–14 ray path, the P-wave velocity decreased along that path after 224 min and the amplitude after 200 min. When compared to the initial P-wave velocity and the resistivity in zone 2, the resistivity increased more than 1.9 Ω.m as the CO_2 saturation was 4.8%. The resistivity change was slightly faster than for the P-wave velocity change when the front of migrating CO_2 reached this ray path.

By comparing changes in P-wave velocity and amplitude while CO_2 was injected into water-saturated sandstone, we observed that the time intervals between changes in P-wave velocity and amplitude due to the front of migrating CO_2 reaching a ray path increased towards the upper side of the sample. The results indicate that the change in amplitude was larger than the change in the P-wave velocity due to CO_2 injection. As a result of comparing changes in resistivity and P-wave velocity at the same time while CO_2 was injected, we observed that the magnitudes of the resistivity changes and the CO_2 saturation increased due to the fact that the front of migrating CO_2 reached a ray path as each channel increased towards the upper side of the sample. The results indicate that CO_2 saturation and CO_2 migration can be evaluated as the cause of the time interval change in P-wave velocity if they increase towards the upper side of a sample. Experimental studies will be carried out to measure resistivity and seismic properties using samples with different porosity and pore structure. The study will be undertaken in order to evaluate the relationship between estimated CO_2 saturation and the behaviour of CO_2 migration using a range of different homogeneous Berea sandstones.

Conclusions

Laboratory experiments were conducted to simultaneously measure combined resistivity and seismic tomography while injecting supercritical CO_2 in water-saturated Berea sandstone.

Our conclusions about our laboratory experiments are as follows:

1. Resistivity increased monotonically, and seismic velocity and amplitude were reduced drastically during the injection of CO_2, suggesting this possibility as a monitoring method for CO_2 underground storage sites.
2. Seismic tomography results depend strongly on the velocity reductions caused by CO_2 injection. The results show that high-resolution seismic methods could be applied to evaluate the behaviour of CO_2 migration for CO_2 monitoring.
3. P-wave velocity became less sensitive when the CO_2 saturation was over ~20%, while the resistivity kept increasing with an increase in CO_2 saturation. The result indicates that the saturation estimation from resistivity can effectively complement CO_2 saturation estimation from seismic velocity variations.
4. By joint interpretation of CO_2 saturation from resistivity and seismic tomography we were able to estimate CO_2 distribution and injected CO_2 behaviour in a sample. The result suggests that combined resistivity and seismic surveys can be applied to simultaneously evaluate CO_2 saturation and CO_2 migration.

In the future, experimental studies will be carried out to estimate CO_2 saturation from P-wave velocity based on the theory of Gassmann fluid substitution with the purpose of better understanding the prediction of CO_2 saturation from resistivity and P-wave velocity. Additionally, such studies will evaluate the relationship between estimated CO_2 saturation and the behaviour of CO_2 migration using reconstructed P-wave velocity images. To better understand the residual (immobile) trapping mechanism, laboratory experiments will be conducted to measure the monitoring with resistivity and P-wave velocity during the imbibition (water injection) stage. This study will be conducted to evaluate residual trapped CO_2 saturation using resistivity and P-wave velocity.

Acknowledgements

This research work was sponsored by the Ministry of Education, Science, Sports and Culture, Grant-in-Aid for "Research of storage quality and quantitative evaluation technology for injected CO_2 in saline aquifer storage".

References

Archie, G. E., 1942, The electrical resistivity log as an aid in determining some reservoir characteristic: *Petroleum Technology*, **5**, 54–62.

Arts, R., Elsayed, R., van der Meer, L., Eiken, O., Ostmo, S., Chadwick, A., Kirby, G., and Zinszner, B., 2002, Estimation of the mass of injected CO_2 at Sleipner using time-lapse seismic data: 64th EAGE meeting, Florence, paper H016.

Arts, R., Eiken, O., Chadwick, A., Zweigel, P., van der Meer, L., and Kirby, G., 2004, Seismic monitoring at the Sleipner underground CO_2 storage site (North Sea), *In* Baines, S. J. and Worden, R. H. (Eds), Geological storage of CO_2 for emissions reduction: *Geological Society, London, Special Publication*, **233**, 181–191.

Bunge, R., 2000, Midale reservoir fracture characterization using integrated well and seismic data, Weyburn Field, Saskatchewan: unpubl. M.Sc. thesis, Colorado School of Mines, 204p.

Daley, T. M., Myer, L. R., Peterson, J. E., Majer, E. L., and Hoversten, G. M., 2007, Time-lapse crosswell seismic and VSP monitoring of injected CO_2 in a brine aquifer: *Environmental Geology*, **54**, 1657–1665. doi:10.1007/s00254-007-0943-z

Davis, T. L., Terrell, M. J., Benson, R. D., and Kendall, R. R., 2002, Seismic monitoring of the CO_2 flood at Weyburn Field, Saskatchewan, Canada: SEG Annual Convention, Utah Extended Abstracts.

Gassmann, F., 1951, Elastic waves through a packing of spheres: *Geophysics*, **16**, 673–685. doi:10.1190/1.1437718

Kim, J. W., Nakatsuka, Y., Xue, Z., and Matsuoka, T., 2009, Monitoring CO_2 injected into water-saturated sandstone with P-wave velocity and resistivity: Proceedings of the 9th international symposium on SEGJ 2009, Sapporo, Japan, Extended Abstracts.

Lei, X.-L., and Xue, Z., 2009, Ultrasonic velocity and attenuation during CO_2 injection into water-saturated porous sandstone: Measurements using difference seismic tomography: *Physics of the Earth and Planetary Interiors*, **176**, 224–234. doi:10.1016/j.pepi.2009.06.001

Nakatsuka, Y., Xue, Z., Yamada, Y., and Matsuoka, T., 2008, Experimental study on monitoring and quantifying of injected CO_2 from resistivity measurement in saline aquifer storage: Proceedings 9th International Conference on Greenhouse Gas Control Technologies (GHGT-9), 2211–2218.

Nakatsuka, Y., Kim, J. W., Xue, Z., Yamada, Y., Matsuoka, T., and Kubota, K., 2009, Quantitative estimation of CO_2 saturation in saline aquifer storage based on resistivity data: Proceedings of the 9th international symposium on SEGJ 2009, Sapporo, Japan, Extended Abstracts.

Onishi, K., Ishikawa, Y., Yamada, Y., and Matsuoka, T., 2006, Measuring electric resistivity of rock samples injected with gas, liquid and super-critical CO_2: Proceedings of the 10th international symposium on RAEG 2006, KIGAM, Korea, 1–8.

Saito, H., Azuma, H., Nobuoka, D., Tanase, D., and Xue, Z., 2006, Time-lapse crosswell seismic monitoring of CO_2 at an onshore aquifer, Nagaoka, Japan: Co-published paper – *Exploration Geophysics*, **37**, 30–36; *Butsuri-Tansa*, **57**, 30–36; *Mulli-Tamsa*, **7**, 30–36. doi:10.1071/EG06030

Xue, Z., and Lei, X.-L., 2006, Laboratory study of CO_2 migration in water-saturated anisotropic sandstone, based on P-wave velocity imaging: Co-published paper – *Exploration Geophysics*, **37**, 10–18; *Butsuri-Tansa*, **59**, 10–18; *Mulli-Tamsa*, **9**, 10–18. doi:10.1071/EG06010

Xue, Z., and Ohsumi, T., 2004*a*, Laboratory measurement of gas permeability and P-wave velocity by CO_2 injection in two porous sandstones during CO_2 flooding: *Journal of the Mining and Materials Processing Institute of Japan*, **120**, 91–98. doi:10.2473/shigentosozai.120.91

Xue, Z., and Ohsumi, T., 2004*b*, Seismic wave monitoring of CO_2 migration in water-saturated porous sandstone: Co-published paper – *Exploration Geophysics*, **35**, 25–32; *Butsuri-Tansa*, **57**, 25–32; *Mulli-Tamsa*, **7**, 25–32. doi:10.1071/EG04025

Xue, Z., and Ohsumi, T., 2005, Experimental studies on seismic monitoring of CO_2 geological sequestration: *Journal of the Japanese Association of Groundwater Hydrology*, **47**, 29–44.

Xue, Z., and Watanabe, J., 2008, Time Lapse Well Logging to Monitor the Injected CO_2 at the Nagaoka Pilot Site: *Journal of the Mining and Materials Processing Institute of Japan*, **124**, 68–77.

Xue, Z., Ohsumi, T., and Koide, H., 2002, Laboratory measurement of seismic wave velocity by CO_2 injection in two porous sandstones, *In* Gale, J. J. and Kaya, Y. (Eds), Proceedings of the 6th International Conference on Greenhouse Gas Control Technologies (GHGT-6), 359–364.

Xue, Z., Tanase, D., Saito, H., Nobuoka, D., and Watanabe, J., 2005, Time-lapse crosswell seismic tomography and well logging to monitor the injected CO_2 in an onshore aquifer, Nagaoka, Japan: 75th Annual International Meeting of the Society of Exploration Geophysicists, Expanded Abstracts, 1433–1436.

Xue, Z., Tanase, D., and Watanabe, J., 2006, Estimation of CO_2 saturation from time-lapse CO_2 well logging in an onshore aquifer, Nagaoka, Japan: Co-published paper – *Exploration Geophysics*, **37**, 19–29; *Butsuri-Tansa*, **59**, 19–29; *Mulli-Tamsa*, **9**, 19–29. doi:10.1071/EG06019

Manuscript received 14 October 2010; revised manuscript received 10 November 2010; accepted 13 December 2010.

탄성파 및 비저항 동시측정에 의한 수포화 암석시료에 주입된 CO_2 모니터링 및 탐지

김종욱 [1], Toshifumi Matsuoka[1], Ziqiu Xue[2]

1 교토대학 대학원 공학연구과 도시사회공학 전공
2 지구환경산업기술연구기관(RITE)

요 약: 전기 및 탄성파 탐사를 이용한 이산화탄소 지중저장의 모니터링의 기초연구로써, 수포화 암석시료에 CO_2주입시 비저항과 P파속도를 측정하였다. 암석시료는 Berea사암이며, CO_2는 초임계상태(10 MPa, 40 ºC)로 주입하였다. 초임계 CO_2주입에 의해 비저항의 증가 및 P파속도와 진폭이 감소하였다. P파 속도 토모그램은 암석시료에 주입한 초임계 CO_2의 거동양상을 보여주었다. 비저항과 탄성파속도는 CO_2거동 모니터링하는데 유용하다. 그러나 P파 속도는 비저항 변화에 비해 CO_2포화도가 20% 이상 일때 변화를 보이지 않았다. 비저항으로부터 CO_2포화도 예측은 탄성파 속도로부터 CO_2포화도 예측의 어려움을 보완할 수 있다. 비저항과 탄성파 속도의 동시측정에 의해 암석시료에 주입한 초임계 CO_2 거동 및 CO_2포화도 분포를 예측할 수 있다.

주요어: 이산화탄소(CO_2) 지중저장, Berea 사암, CO_2 포화도, P 파 속도, 비저항, 탄성파토모그래피

弾性波と比抵抗の同時測定による水飽和砂岩に注入された CO_2 モニタリング及び探知

金 鍾旭 [1]・松岡俊文 [1]・薛 自求 [2]

1 京都大学大学院工学研究科都市社会工学専攻
2 地球環境産業技術研究機構(RITE)

要 旨: 電気及び弾性波探査を利用した二酸化炭素地中貯留のモニタリングの基礎研究として、水飽和砂岩に CO_2 注入時の比抵抗と P 波速度の測定実験を実施した。岩石試料はベリア砂岩である。CO_2 は超臨界状態(10 MPa, 40 °C)で注入した。超臨界 CO_2 の注入によって、比抵抗の増加及び P 波の伝搬速度と振幅が減少した。弾性波トモグラフィの結果は砂岩試料に注入された超臨界 CO_2 挙動を示した。従って、比抵抗と弾性波速度は CO_2 挙動のモニタリングにおいて有用である。しかし、P 波速度は比抵抗と比較して、CO_2 飽和度が 20% 以上の時に変化が見えなかった。以上より、比抵抗を用いた CO_2 飽和度の予測は、弾性波速度による CO_2 飽和度の予測の難しさを効果的に補うことができることが示される。比抵抗と弾性波速度 を結合することによって、砂岩試料に注入された超臨界 CO_2 挙動及び CO_2 飽和度分布が予測できた。

キーワード: 二酸化炭素(CO_2)地中貯留, ベリア砂岩, CO_2 飽和度, P 波速度, 比抵抗, 弾性波トモグラフィ